

Global minima of Al_N , Au_N and Pt_N , $N \leq 80$, clusters described by Voter-Chen version of embedded-atom potentials

Ali Sebetci*

*Department of Computer Engineering,
Çankaya University, 06530 Balgat Ankara, Turkey*

Ziya B. Güvenc†

*Department of Electronic and Communication Engineering,
Çankaya University, 06530 Balgat Ankara, Turkey*

(Dated: May 3, 2021)

Abstract

Using the basin-hopping Monte Carlo minimization approach we report the global minima for aluminium, gold and platinum metal clusters modelled by the Voter-Chen version of the embedded-atom model potential containing up to 80 atoms. The virtue of the Voter-Chen potentials is that they are derived by fitting to experimental data of both diatomic molecules and bulk metals simultaneously. Therefore, it may be more appropriate for a wide range of the size of the clusters. This is important since almost all properties of the small clusters are size dependent. The results show that the global minima of the Al, Au and Pt clusters have structures based on either octahedral, decahedral, icosahedral or a mixture of decahedral and icosahedral packing. The 54-atom icosahedron without a central atom is found to be more stable than the 55-atom complete icosahedron for all of the elements considered in this work. The most of the Al global minima are identified as some fcc structures and many of the Au global minima are found to be some low symmetric structures, which are both in agreement with the previous experimental studies.

PACS numbers: 36.40.-c; 61.46.+w

Keywords: Atomic clusters; Pt clusters; cluster structures; molecular dynamics; embedded atom method; basin-hopping algorithm.

*Electronic address: asebetci@cankaya.edu.tr

†Electronic address: guvenc@cankaya.edu.tr

I. INTRODUCTION

Since Richard Feynman's famous challenging talk *There's Plenty of Room at the Bottom* in 1959 [1], many scientists all over the world are still studying on the investigation and fabrication of nanometer scale (10^{-9} m) structures and devices. In his talk, he challenged scientists to develop a new field of study where devices and machines could be constructed from components consisting of a small number (tens or hundreds) of atoms. The use of metal and semiconductor clusters as components of nanodevices is one of the most important reasons which explains why there are considerable theoretical and experimental interest in the study of gas phase and supported metal clusters in the last few decades [2, 3, 4, 5, 6]. Due to their finite size, these small particles may have totally different structures and material properties than their bulk crystalline forms. Furthermore, these properties may sometimes change drastically whenever a single atom is added to or removed from the cluster [7]. A systematic study of evolution of these properties with size allows elucidation of the transition from the molecular structure to condensed matter phase. Clusters, in particular metal clusters, play an important role in many chemical reactions as catalysts, as well. The structure of small metal clusters in a reaction can have a major effect on the rate of formation of products [8].

In this study, using the basin-hopping [9] Monte Carlo minimization approach we report the global minima for aluminium, gold and platinum metal clusters modelled by the Voter-Chen [10] version of the embedded-atom model (EAM) [11] potential containing up to 80 atoms. The virtue of the Voter-Chen potentials is that they are derived by fitting to experimental data of both diatomic molecules and bulk metals simultaneously. Therefore, it may be more appropriate for a wide range of the size of the clusters. This is important since almost all properties of the small clusters are size dependent.

This paper is organized as follows: The interaction potential and the computational procedure will be discussed in Section II. Results and discussions are presented in Section III, and conclusions are given in Section IV.

II. COMPUTATIONAL METHODS

A. The Voter-Chen Potential

In any N -scaling energy expression, the total energy, E_{tot} of a system of N atoms can be written as a sum

$$E_{tot} = \sum_i^N E_i. \quad (1)$$

In the EAM, the configuration energy E_i of each atom i is represented as

$$E_i = \frac{1}{2} \sum_{j \neq i} \phi_{ij}(r_{ij}) + F_i(\bar{\rho}_i), \quad (2)$$

where F_i is the embedding term, ϕ_{ij} is the pairwise-addition part of the interaction between atoms i and j , r_{ij} is the distance between atoms i and j , and $\bar{\rho}_i$ is the total "host" electron density at the position of atom i :

$$\bar{\rho}_i = \sum_{j \neq i} \rho_j(r_{ij}). \quad (3)$$

The sums over neighboring atoms j are limited by the range of the cutoff for ϕ and ρ , which is approximately 5 Å for the metals considered in this work. Key to the EAM is the nonlinearity of the function $F(\bar{\rho})$ which provides a many-body contribution to the energy. If F were purely linear, the two terms in Eq.2 could be collapsed to give a simple pair potential. Thus, a nonlinear $F(\bar{\rho})$ provides a many-body contribution to the energy. Because $\bar{\rho}_i$ depends only on scalar distances to neighboring atoms, the many-body term has no angular dependence. Nonetheless, this spherically symmetric, many-body interaction is quite important.

All the parameters in the Voter and Chen model were determined by minimizing the root-mean-square deviation (χ_{rms}) between the calculated and experimental values of three elastic constants (C_{11} , C_{12} , and C_{44}), the unrelaxed vacancy formation energy (E_{vac}^f) of the bulk metals (Al, Au and Pt), and of the bond length (R_e) and bond strength (D_e) of their diatomic molecules.

B. The Basin-Hopping Algorithm

Two new and more successful algorithms have been developed within the last two decades to search the global minimum of an energy landscape, which are different than the traditional

random search and simulated annealing techniques: basin-hopping and genetic algorithms. The genetic algorithm is a search based on the principles of natural evolution [12], while the basin-hopping approach belongs to the family of hypersurface deformation methods [13] where the energy is transformed to a smoother surface. The basin-hopping algorithm which we have used in the present work is based upon Li and Scheraga's [16] Monte Carlo (MC) minimization, and it has been developed and employed for several systems by Doye and Wales [9, 14, 15]. In the basin-hopping algorithm, the transformed potential energy surface (PES), $\tilde{E}(\mathbf{X})$, is defined by $\tilde{E}(\mathbf{X}) = \min\{E(\mathbf{X})\}$, where \mathbf{X} represents the vector of atomic coordinates and *min* signifies that an energy minimization is performed starting from \mathbf{X} . Unlike many PES transformations, this basin-hopping transformation guarantees to preserve the identity of the global minimum. The topography of the transformed surface is that of a multi-dimensional staircase (a set of interpenetrating staircases with plateaus corresponding to the basins of attraction of each minimum). Since the barriers between the local minima are removed in the transformed PES, vibrational motions within the well surrounding a minimum are removed. In addition, transitions from one local minimum to another in the transformed PES can occur at any point along the boundary between these local minima, whereas on the untransformed surface transitions can occur only when the system passes through the transition state. Consequently, on $\tilde{E}(\mathbf{X})$, the system can hop directly between the basins; hence it is the name of this transformation.

We have used the GMIN [17] program in our simulations to locate the lowest energy structures of the Voter-Chen Al, Au and Pt clusters. The MC runs have been started with the configurations which are the global minima of the Morse clusters. For a given size, as the interaction range of the Morse potential changes, the global minimum varies. Different global minima for different interaction ranges of the Morse potential were reported up to 80-atom clusters before [18, 19]. We have reoptimized all these Morse global minima by performing several MC runs of 100,000 steps of each.

III. RESULTS AND DISCUSSION

A. Aluminium Clusters

It goes back to the middle of the 1980s that a number of theoretical studies of Al clusters have been carried out by different groups [20, 21, 22, 23, 24, 25, 26, 27, 28, 29, 30, 31, 32, 33, 34, 35, 36, 37, 38, 39]. These studies range from the simple jellium model [20] where the cluster geometry is ignored, to a number of models where the geometry explicitly enters into the picture including semiempirical molecular orbital calculations [21], quantum molecular dynamics [26, 27, 28, 29, 31], quantum-mechanical calculations based on quantum-chemical [22, 23, 24] and density-functional [25, 26, 27, 28, 29, 30, 31, 32, 33] theories (DFT) within local density or local spin-density approximations, molecular dynamics and Monte Carlo simulations based on empirical model potentials [34, 35, 36, 37, 38, 39]. Especially the icosahedral Al_{13} has been studied intensively [24, 32]. The most recent and more extensive density-functional calculations have been presented by Ahlrichs and Elliott [29] and by Rao and Jena [33] in 1999. These studies focused both on electronic and structural properties of neutral and ionized Al clusters up to 15 atoms, respectively. On the other hand, while the empirical model potential studies [34, 35, 36, 37, 38, 39] cannot calculate the electronic properties of the clusters, it is possible to search PES of higher sized clusters with them since they are computationally much less demanding than *ab initio* calculations. In these model potential studies carried out by random search, simulated annealing or genetic algorithms, Al clusters are described by an empirical many-body potential [34], two-plus-three body Murrell-Mottram potential [35, 36, 37], Gupta [38] or Sutton-Chen [39] potentials. Similarly, the experimental studies on Al clusters [40, 41, 42, 43, 44, 45, 46, 47, 48, 49, 50, 51] go back to the middle of the 1980s. It is known that while the electronic factors determine cluster stability for alkali metal clusters [52], packing and surface energy effects dominate on the structure of alkaline earth elements, such as calcium and strontium [51]. Aluminium places at a central position between the regimes of electronic and geometric shells [45]. Martin's mass spectroscopic studies [51] have shown that Al clusters with up to a few hundred atoms have face-centred cubic (fcc) packing structures. These experimental interpretations have been confirmed by theoretical calculations using empirical potentials [38] and DFT [29]. Jarrold and Bower have performed experiments on smaller Al clusters which enabled them

to determine the topologies of clusters with tens of atoms [41].

We have reported the total energies (E), the point groups (PG), and the structural assignments (SA) (whenever possible) of the global minima for the Al clusters up to 80 atoms described by the Voter-Chen potential in Table I. The point groups of the structures are determined with OPTIM program [17]. Symmetry elements are diagnosed when rotation and reflection operators produce the same geometry (correct to 0.001) in each Cartesian coordinates. The energies and the second finite differences in energies

$$D_2E(N) = E_l(N + 1) + E_l(N - 1) - 2E_l(N) \quad (4)$$

are plotted in Figs. 1(a) and (b), respectively. Following Northby *et al.* [53] and Lee and Stein [54], the function,

$$E_0 = aN + bN^{2/3} + cN^{1/3} + d, \quad (5)$$

is fitted to the energies given in Table I, and it is subtracted from the energies of the clusters in order to emphasize the size dependence. In this polynomial function, a describes the volume, b surface, c edge, and d the vertex contributions to the energy. D_2E is generally correlated with the magic numbers observed in mass spectra. Clusters are particularly abundant at magic number sizes in mass spectra since they are the most stable ones [55].

The triangulated polyhedral structures of the Al₇-Al₈₀ global minima are illustrated in Fig. 2. The structures for the first seven Al_N clusters ($N = 2 - 8$) are similar to those obtained by other empirical potentials for aluminum [36, 39] and other metals [14, 56]. Al₃ forms an equilateral triangle, Al₄ a tetrahedron, Al₅ a trigonal bipyramid, Al₆ an octahedron, Al₇ a pentagonal bipyramid, and Al₈ is a bicapped octahedron. All of these structures are located as the global minima of Au and Pt clusters in the present work, too. Al₉ can be described as a three capped trigonal prisms and Al₁₀ is a hexadecahedron, which are the same with Joswig and Springborg's calculations of Al clusters employed by Sutton-Chen potential [39]. Structures of the Al clusters with $N = 11 - 14$ atoms are icosahedral. The Al₁₅ is the sixfold icositetrahedron. The 16- and 17-atom Al clusters involve a mixture of decahedral and icosahedral stacking sequences. The Al₁₉ is a double icosahedron. In the size range of $N = 20 - 36$, all clusters have face-sharing icosahedral (fsI) structures possessing generally low symmetries. Above the size of 36, the most of the Al clusters are fcc packed. This is consistent with Martin's experimental study [51] with the exceptions of the 40-, 51-, 53- and 54-atom uncentred icosahedral (ucI) structures, the 55-atom centred icosahedron,

and the 60-, 64-, 67-, 72-, 73- and 74-atom decahedral (dec) structures. As a result the total number of fcc Al clusters having more than 36 atoms is 26.

It can be seen from both of the Figs. 1(a) and (b) that the most stable structure occurs at size 13 which corresponds to complete Mackay icosahedra [57]. The other relatively more stable structures with respect to their neighboring sizes are $N=38$, 50, 54, 61, 68 and 75 corresponding to truncated octahedron, twinned truncated octahedron, uncentred icosahedra [58], and some other three fcc structures, respectively.

B. Gold Clusters

Gold nanoparticles are a fundamental part of recently synthesized novel nanostructured materials and devices [59, 60, 61]. Structural characterization using a variety of experimental techniques can be performed on Au clusters [62, 63, 64, 65, 66]. Experiments suggest that gold nanoclusters with diameters of 1-2 nm, corresponding to aggregates with $N=20$ -200 atoms, are amorphous [62, 63]. The theoretical studies on gold nanoclusters change from empirical MD or MC simulations using EAM [67], Gupta [68], Sutton-Chen [14] and Murrell-Mottram [69] potentials to some first-principle calculations using DFT [70, 71], generalized gradient approximation [72], spin-polarized Becke-Lee-Yang-Parr functional [73], and Hartree-Fock and post Hartree-Fock levels [74].

We have reported the total energies (E), the point groups (PG), and the structural assignments (SA) (whenever possible) of the global minima for the gold clusters of $N=2$ -80 atoms described by the Voter-Chen potential in Table II. The energies and the second finite differences in energies are plotted in Figs. 3(a) and (b), respectively. The triangulated polyhedral structures of the Au_7 - Au_{80} global minima are illustrated in Fig. 4. In our calculations we have found that Au_9 - Au_{14} clusters are icosahedral. The 13-atom icosahedron has been reported as the lowest energy structure of a Au_{13} cluster by some of the previous empirical studies [14, 69] as well, although they have presented some other structures for some of the gold clusters in this size range. However, the icosahedron is not the global minimum in the first principle calculations of Wang et al. [71]. In addition, in many of the *ab initio* studies the lowest energy structures of the small clusters are found to be some planar forms [70, 71, 72]. This is because of the fact that since the empirical many body methods are lack of directionality, these potentials favor more compact, spherically symmet-

ric structures. However, this discrepancy between the first principle and empirical methods vanishes when the cluster size increases. In our results the global minima of Au₁₅, Au₁₆, Au₁₈, and Au₁₉ are the same as those of the corresponding Al clusters. Similar to the Al clusters, in the size range of $N = 20 - 36$, all gold clusters have fsl structures. The 37-atom cluster has a mixture of decahedral and icosahedral morphologies. The 38-atom cluster is a truncated octahedron. We have found only two more fcc structures (at $N = 61$ and $N = 79$) in the global minima of Au clusters above this size. In agreement with many of the previous theoretical calculations, the Au₅₅ is not a icosahedron in our calculations too, although 52-, 53-, and 54-atom Au clusters are ucI. For the size range of $N = 64 - 79$, the dominant structural motif is the decahedral morphology. While the 64-, 71-, and 75-atom clusters have perfect decahedral structures, the 66-, 72-, 73-, 74-, 76-, and 77-atom clusters have some icosahedral deficiencies on their decahedral backbones. Our results for the Au clusters are in agreement with the experimental suggestion that gold nanoclusters with $N=20-200$ atoms are amorphous [62, 63] since the most of the structures reported in the present work have low symmetry (i.e., C_s). Fig. 3(b) suggests that the most stable structures occur at sizes of 13, 30, 40, 54, 66, 73, 75 and 77. The 38-atom truncated octahedron does not seem as a magic number of the Au clusters, instead a 40-atom amorphous structure is more stable. For the higher sizes, decahedral structures and mixtures of decahedral and icosahedral staking sequences become more stable than the others, except the 54-atom uncentred icosahedron.

C. Platinum Clusters

We have reported before the lowest energy structures, the numbers of stable isomers, growth pathways, probabilities of sampling the basins of attraction of the stable isomers, and the energy spectrum-widths which are defined by the energy difference between the most and the least stable isomers of Pt₂-Pt₂₁ clusters [56] and the global minima of Pt₂₂-Pt₅₆ clusters [58]. Since all relevant literature of platinum clusters can be found in those studies, we do not repeat them here once more. We have reported the total energies (E), the point groups (PG), and the structural assignments (SA) of the global minima of Pt clusters described by the Voter-Chen potential for $N \leq 80$ atoms in Table III. The energies and the second finite differences in energies are plotted in Figs. 5(a) and (b), respectively. The triangulated polyhedral structures of the Pt₇-Pt₈₀ global minima are illustrated in Fig. 6.

The lowest energy structures of the Pt clusters are more similar to those of the Au clusters than those of the Al clusters. All the global minima of Au and Pt clusters are identical for $N \leq 17$. The 18-atom Pt cluster does not have the decahedral morphology of the Au_{18} cluster. In the size range of $N=19-38$, the most of the Pt clusters have uCI structures which are similar to the cases for both Al and Au clusters. In this size range, 12 Pt clusters have identical structures with the corresponding Au clusters (i.e., at the sizes of 19-21, 26, 28-30, 32, 33, 36-38). The main differences between the Au and Pt clusters occur at the sizes of 41, 50, 51, 55, 70, 74, 76, 78, and 80: the 41-atom Pt cluster has a mixture of decahedral and icosahedral morphologies, the 50-atom Pt cluster is a twinned truncated octahedron, the 51-atom cluster is an uncentred icosahedron missing three surface atoms, the 55-atom cluster is a complete Mackay icosahedron, the 70-, 74-, and 76-atom clusters are some decahedrons and finally the 78- and 80-atom Pt clusters have a mixture of decahedral and icosahedral staking sequences. For the higher sizes, while Pt clusters prefer fully decahedral structures, the Au clusters favor structures involving a mixture of decahedral and icosahedral staking sequences (see the sizes of 70, 74, and 76). When the normalized energy (Fig. 5(a)) and second finite difference in energy plots (Fig. 5(b)) of the Pt clusters are considered, it can be seen that the most stable sizes are 13, 38, 50, 54, 61, 68, and 75. Interestingly, these magic numbers are more similar to those of the Al than those of the Au clusters.

IV. CONCLUSIONS

In the present study, we have reported the global minima of Al, Au and Pt clusters up to 80 atoms described by the Voter-Chen version of the EAM potential in a basin-hopping MC geometry minimization technique. The results show that the global minima of the Al, Au and Pt clusters have structures based on either fcc, decahedral, icosahedral or a mixture of decahedral and icosahedral packing. The 54-atom icosahedron without a central atom is found to be more stable than the 55-atom complete icosahedron for all of the elements considered in this work. The most of the Al global minima are identified as some fcc structures as the previous experimental studies suggest. Many of the Au global minima are found to be some low symmetric structures, which is also in some agreement with the experimental studies of the Au clusters. Although many of the Pt global minima are identical with the global minima of the corresponding Au clusters, the most stable sizes

of the Pt clusters occur at the same sizes of the Al clusters.

-
- [1] R.P. Feynman, Talk at the annual meeting of the American Physical Society at the California Institute of Technology (Caltech), December 29th, (1959).
- [2] H. Haberland (Ed.), *Clusters of Atoms and Molecules* (Springer, Berlin, 1994); and references therein.
- [3] G. Schmid (Ed.), *Clusters and Colloids* (VCH, Weinheim, 1994); and references therein.
- [4] T.P. Martin (Ed.), *Large Clusters of Atoms and Molecules* (Kluwer, Dordrecht, 1996); and references therein.
- [5] J. Jellinek (Ed.), *Theory of Atomic and Molecular Clusters* (Springer, Berlin, 1999); and references therein.
- [6] Roy L. Johnston, *Atomic and Molecular Clusters* (Taylor and Francis, London, 2002); and references therein.
- [7] W. Eberhardt, Surf. Sci. 500, 242 (2002).
- [8] J. Jellinek and Z.B. Güvenc, Z. Phys. D 26, 110 (1993); J. Jellinek and Z.B. Güvenc, in *The Synergy Between Dynamics and Reactivity at Clusters and Surfaces* (L.J. Farrugia, Ed. Kluwer, Dordrecht, 1995, p.217).
- [9] D.J. Wales and J.P.K. Doye, J. Phys. Chem. A 101, 5111 (1997).
- [10] A.F. Voter, Los Alamos Unclassified Technical Report #LA-UR 93-3901 (1993).
- [11] M.S. Daw and M.I. Baskes, Phys. Rev. B 29, 6443 (1984).
- [12] D.E. Goldberg, *Genetic Algorithms in Search, Optimisation and Machine Learning* (Addison-Wesley, Reading, MA, 1989).
- [13] F.H. Stillinger and T.A. Weber, J. Stat. Phys. 52, 1429 (1988).
- [14] J.P.K. Doye, and D.J. Wales, New J. Chem. 733 (1998).
- [15] J.P.K. Doye, Phys. Rev. B 68(19), 195418 (2003); and references therein.
- [16] Z. Li and H.A. Scheraga, Proc. Natl. Acad. Sci. USA, 84, 6611 (1987).
- [17] <http://www-wales.ch.cam.ac.uk/software.html>.
- [18] J.P.K. Doye, D.J. Wales, and R.S. Berry, J. Chem. Phys. 103, 4234 (1995).
- [19] J.P.K. Doye and D.J. Wales, J. Chem. Soc. Faraday Trans. 93, 4233 (1997).
- [20] M.Y. Chou and M.L. Cohen, Phys. Lett. A 113, 420 (1986).
- [21] K. Jug, H.P. Schluff, H. Kupka, and R. Iffert, J. Comput. Chem. 9, 803 (1988).

- [22] G. Pacchioni and J. Koutecky, *Ber. Bunsenges. Phys. Chem.* 88, 242 (1984).
- [23] T.H. Upton, *J. Phys. Chem.* 90, 754, (1986); *Phys. Rev. Lett.* 56, 2168 (1986).
- [24] L.G.M. Petersson, C.W. Bauschlicher, Jr., and T. Halicioglu, *J. Chem. Phys.* 87, 2205 (1987).
- [25] H.P. Cheng, R.S. Berry, and R.L. Whetten, *Phys. Rev. B* 43, 10647 (1991).
- [26] J.Y. Yi, D.J. Oh, and J. Bernhole, *Phys. Rev. Lett.* 67, 1594 (1991).
- [27] R.O. Jones, *Phys. Rev. Lett.* 67, 224, (1991); *J. Chem. Phys.* 99, 1194 (1993).
- [28] J. Akola, H. Hakkinen, and M. Manninen, *Phys. Rev. B* 58, 3601 (1998).
- [29] R. Ahrichs and S.D. Elliott, *Phys. Chem. Chem. Phys.* 1, 13 (1999).
- [30] S.N. Khanna and P. Jena, *Phys. Rev. Lett.* 69, 1664 (1992).
- [31] X.G. Gong and V. Kumar, *Phys. Rev. Lett.* 70, 2078 (1993).
- [32] E.B. Krissinel and J. Jellinek, *Int. J. Quantum Chem.* 62, 185 (1997).
- [33] B.K. Rao and P. Jena, *J. Chem. Phys.* 111, 1890 (1999).
- [34] Z. El-Bayyari and Ş. Erkoç, *Phys. Status Solidi B* 170, 103 (1992).
- [35] R.L. Johnston and J.-Y. Fang, *J. Chem. Phys.* 97, 7809 (1992)
- [36] L.D. Lloyd and R.L. Johnston, *Chem. Phys.* 236, 107 (1998).
- [37] L.D. Lloyd, R.L. Johnston, C. Roberts, and T.V. Mortimer-Jones, *Chem. Phys. Chem.* 3, 408 (2002).
- [38] G.W. Turner, R.L. Johnston, and N.T. Wilson, *J. Chem. Phys.* 112, 4773 (1999).
- [39] J.-O. Joswig and M. Springborg, *Phys. Rev. B* 68, 085408 (2003).
- [40] D.M. Cox, D.J. Trevor, R.L. Whetten, E.A. Rohlfing, and A. Kaldor, *J. Chem. Phys.* 84, 4651 (1986).
- [41] M.F. Jarrold, J.E. Bower, and J.S. Kraus, *J. Chem. Phys.* 86, 3876 (1987).
- [42] L. Hanley, S. Ruatta, and S. Anderson, *J. Chem. Phys.* 87, 260 (1987).
- [43] W.A. Saunders, P. Fayet, and L. Wöte, *Phys. Rev. A* 39, 4400 (1989).
- [44] R.E. Leuchtner, A.C. Harms, and A.W. Castleman, Jr., *J. Chem. Phys.* 91, 2753 (1989); 94, 1093 (1991).
- [45] K.E. Schriver, J.L. Persson, E.C. Honea, and R.L. Whetten, *Phys. Rev. Lett.* 64, 2539 (1990).
- [46] W.A. de Heer, P. Milani, and A. Chatelain, *Phys. Rev Lett.* 63, 2834 (1989).
- [47] G. Ganteför, M. Gausa, K.H. Meiwes-Broer, and H.O. Lutz, *Z. Phys. D* 9, 253 (1988).
- [48] K.J. Taylor, C.L. Pettiette, M.J. Graycraft, O. Chesnovsky, and R.E. Smalley, *Chem. Phys. Lett.* 152, 347 (1988).

- [49] A. Nakajima, K. Hoshino, T. Naganuma, Y. Sone, and K. Kaya, *J. Chem. Phys.* 95, 7061 (1991).
- [50] X. Li, H. Wu, X.B. Wang, and L.S. Wang, *Phys. Rev. Lett.* 81, 1090 (1998).
- [51] T.P. Martin, *Phys. Rep.* 199, 273 (1996).
- [52] W.D. Knight, K. Clemenger, W.A. de Heer, W.A. Saunders, M.Y. Chou, M.L. Cohen, *Phys. Rev. Lett.* 52, 2141 (1984).
- [53] J.A. Northby, J. Xie, D.L. Freeman, J.D. Doll, *Z. Phys. D* 12, 69 (1989).
- [54] J.W. Lee, G.D. Stein, *J. Phys. Chem.* 91, 2450 (1987).
- [55] K. Clemenger, *Phys. Rev. B* 32, 1359 (1985).
- [56] A. Sebetci and Z.B. Güvenç, *Surf. Sci.* 525, 66 (2003).
- [57] A.L. Mackay, *Acta Crystallogr.* 15, 916 (1962).
- [58] A. Sebetci and Z.B. Güvenç, *Eur. Phys. J. D*, 30(1), 71 (2004).
- [59] R.L. Whetten, M.N. Shafiqullin, J.T. Khoury, T.G. Schaaff, I. Vezmar, M.M. Alvarez, A. Wilkinson, *Acc. Chem. Res.* 32(5), 397 (1999).
- [60] J.-M. Nam, C.S. Thaxton, C.A. Mirkin, *Science* 301, 1884 (2003).
- [61] J Liu, T Lee, D.B. Janes, B.L. Walsh, M.R. Melloch, J.M. Woodall, R. Reifengerger, R.P. Andres, *Appl. Phys. Lett.* 77(3), 373 (2000).
- [62] R.N. Barnett, C.L. Cleveland, H. Hakkinen, W.D. Luedtke, C. Yannouleas C, U Landman, *Eur. Phys. J. D* 9(1-4), 95 (1999).
- [63] T.G. Schaaff, M.N. Shafiqullin, J.T. Khoury, I. Vezmar, R.L. Whetten, W.G. Cullen, P.N. First, C. GutierrezWing, J. Ascensio, M.J. JoseYacaman, *J. Phys. Chem. B* 101, 7885 (1997).
- [64] K. Koga, H. Takeo, T. Ikeda, K.I. Ohshima, *Phys. Rev. B* 57, 4053 (1998).
- [65] B. Palpant, B. Prevel, J. Lerme, E. Cottancin, M. Pellarin, M. Treilleux, A. Perez, J.L. Vialle, M. Broyer, *Phys. Rev. B* 57, 1963 (1998).
- [66] V.A. Spasov, Y. Shi, K.M. Ervin, *Chem. Phys.* 262, 75 (2000).
- [67] C.L. Cleveland, W.D. Luedtke, U. Landman, *Phys. Rev. B* 60(7), 5065 (1999).
- [68] I.L. Garzon, K. Michealian, M.R. Beltran, A. Posada-Amarillas, P. Ordejon, E. Artacho, D. Sanchez-Portal, J.M. Soler, *Phys. Rev. Lett.* 81, 1600 (1998).
- [69] N.T. Wilson and R.L. Johnston, *Eur. Phys. J. D* 12, 161 (2000).
- [70] O. D. Häberlen, S.-C. Chung, M. Stener, N. Rsch, *J. Chem. Phys.* 106, 5189 (1997).
- [71] J.L. Wang, G.H. Wang, J.J. Zhao, *Phys. Rev. B* 66(3), Art. No. 035418 (2002).

- [72] H. Häkkinen and U. Landman, *Phys. Rev. B* 62, 2287 (2000).
- [73] H. Grönbech and W. Andreoni, *Chem. Phys.* 262, 1 (2000).
- [74] G. Bravo-Perez, I.L. Garzon, O. Novaro, *J. Mol. Struct.: THEOCHEM* 493, 225 (1999).

TABLE I: Global minima for Al clusters. For each minimum energy (E), point group (PG) and structural assignment (SA) are given if possible. The structural categories are: centred (cI), uncentred (ucI) and face-sharing icosahedral (fsI); face centred cubic packed (fcc); decahedral with n atoms along the decahedral axis (dec(n)); involving a mixture of staking sequences (mix).

N	E (eV)	PG	SA	N	E (eV)	PG	SA
				41	-113.6500	C_{3v}	fcc
2	-1.5443	$D_{\infty h}$		42	-116.5605	C_s	fcc
3	-3.7442	D_{3h}		43	-119.5276	C_s	fcc
4	-6.3998	T_d		44	-122.5599	C_2	
5	-8.9663	D_{3h}		45	-125.6996	C_{2v}	fcc
6	-11.8950	O_h	fcc	46	-128.5274	C_2	
7	-14.5508	D_{5h}		47	-131.4723	C_{2v}	
8	-17.2960	D_{2d}		48	-134.5603	C_2	
9	-20.0965	D_{3h}		49	-137.4842	C_s	
10	-22.8679	D_{4d}		50	-140.8376	D_{3h}	fcc
11	-25.5008	C_{2v}	cI	51	-143.7037	C_{3v}	ucI
12	-28.5274	C_{5v}	cI	52	-146.9402	D_{2h}	fcc
13	-32.0729	I_h	cI	53	-149.9979	C_{5v}	ucI
14	-34.4434	C_{3v}	cI	54	-153.1459	I_h	ucI
15	-37.4486	D_{6d}		55	-155.9151	I_h	cI
16	-40.2857	C_{2v}		56	-158.6939	C_1	
17	-43.1633	D_{4h}	mix	57	-161.8106	C_s	fcc
18	-45.8783	C_{4v}	mix	58	-164.8037	C_{3v}	
19	-48.8299	D_{5h}	cI	59	-167.8936	C_1	fcc
20	-51.7096	D_{2h}	fsI	60	-170.8159	C_{2v}	dec(5)
21	-54.5367	C_s	fsI	61	-174.1955	C_{3v}	fcc
22	-57.5353	C_s	fsI	62	-176.8996	C_s	fcc
23	-60.4193	C_1	fsI	63	-179.9652	C_s	fcc
24	-63.2273	C_s	fsI	64	-183.1181	C_{2v}	dec(5)
25	-66.1897	C_3	fsI	65	-186.0925	C_{2v}	fcc
26	-69.0988	C_1	fsI	66	-189.1802	C_s	fcc
27	-72.0921	C_{2v}	fsI	67	-192.2851	C_{2v}	dec(5)
28	-74.9678	C_s	fsI	68	-195.5431	T_d	fcc
29	-77.8530	C_1	fsI	69	-198.2053	C_1	fcc
30	-80.8463	C_s	fsI	70	-201.5432	C_{2v}	fcc
31	-83.9112	C_s	fsI	71	-204.6298	C_s	fcc
32	-86.8113	C_2	fsI	72	-207.4224	C_{2v}	dec(5)
33	-89.6630	C_1	fsI	73	-210.6064	D_{5h}	dec(5)
34	-92.7060	C_1	fsI	74	-213.7521	C_{5v}	dec(5)
35	-95.7977	D_3	fsI	75	-216.9853	C_s	fcc
36	-98.6907	C_{2v}	fsI	76	-219.6910	C_4	fcc
37	-101.6952	C_{3v}	fcc	77	-222.8998	C_s	fcc
38	-105.1156	O_h	fcc	78	-225.9885	C_s	fcc
39	-107.8211	C_{4v}	fcc	79	-229.1335	D_{3h}	fcc
40	-110.5958	C_1	ucI	80	-231.9938	C_{4v}	fcc

TABLE II: Global minima for Au clusters. For each minimum energy (E), point group (PG) and structural assignment (SA) are given if possible. The structural categories are: centred (cI), uncentred (ucI) and face-sharing icosahedral (fsI); face centred cubic packed (fcc); decahedral with n atoms along the decahedral axis (dec(n)); involving a mixture of staking sequences (mix).

N	E (eV)	PG	SA	N	E (eV)	PG	SA
				41	-138.2008	C_s	fsI
2	-2.2886	$D_{\infty h}$		42	-141.9077	C_4	fsI
3	-5.2797	D_{3h}		43	-145.4197	C_s	
4	-8.8497	T_d		44	-149.0400	C_s	
5	-12.1736	D_{3h}		45	-152.6610	C_s	
6	-15.8281	O_h	fcc	46	-156.2059	C_s	
7	-19.1505	D_{5h}		47	-159.8067	C_s	
8	-22.4326	D_{2d}		48	-163.4242	C_s	
9	-25.7507	C_{2v}	cI	49	-167.0450	C_s	
10	-29.1712	C_{3v}	cI	50	-170.5777	C_s	
11	-32.4968	C_{2v}	cI	51	-174.1304	C_s	
12	-36.0088	C_{5v}	cI	52	-177.9191	C_{2h}	ucI
13	-40.1043	I_h	cI	53	-181.7385	C_{5v}	ucI
14	-42.9943	C_{3v}	cI	54	-185.5635	I_h	ucI
15	-46.6960	D_{6d}		55	-188.6971	C_s	
16	-50.1275	C_s		56	-192.2661	C_s	
17	-53.5914	C_s		57	-195.8573	C_s	
18	-56.9242	C_{4v}	mix	58	-199.4305	C_s	
19	-60.3352	D_{5h}	cI	59	-202.9304	C_s	
20	-63.7463	C_{2h}	fsI	60	-206.6851	C_s	
21	-67.2933	C_s	fsI	61	-210.3464	C_{3v}	fcc
22	-70.9625	C_s	fsI	62	-213.9025	C_s	
23	-74.5236	C_s	fsI	63	-217.5417	C_{2v}	
24	-77.9539	C_s	fsI	64	-221.2716	C_{2v}	dec(5)
25	-81.3036	C_s	fsI	65	-224.9052	C_s	
26	-84.8046	C_s	fsI	66	-228.6560	C_s	mix
27	-88.4414	C_s	fsI	67	-232.1324	C_s	
28	-92.0749	C_s	fsI	68	-235.8811	C_s	
29	-95.5729	C_s	fsI	69	-239.5284	C_s	
30	-99.2318	C_{3v}	fsI	70	-243.1537	C_s	
31	-102.5796	C_s	fsI	71	-246.8875	C_{2v}	dec(5)
32	-106.1560	D_{2d}	fsI	72	-250.5921	C_s	mix
33	-109.6664	C_s	fsI	73	-254.3504	C_s	mix
34	-113.2711	C_s	fsI	74	-257.8233	C_s	mix
35	-116.8575	C_s	fsI	75	-261.6719	D_{5h}	dec(5)
36	-120.4893	C_{2v}	fsI	76	-265.2637	C_s	mix
37	-124.0150	C_{2v}	mix	77	-269.0221	C_s	mix
38	-127.6334	O_h	fcc	78	-272.4326	C_s	
39	-131.1339	C_s	fsI	79	-276.1669	D_{3h}	fcc
40	-134.8451	C_s	fsI	80	-279.8123	C_s	

TABLE III: Global minima for Pt clusters. For each minimum energy (E), point group (PG) and structural assignment (SA) are given if possible. The structural categories are: centred (cI), uncentred (ucI) and face-sharing icosahedral (fsI); face centred cubic packed (fcc); decahedral with n atoms along the decahedral axis (dec(n)); involving a mixture of staking sequences (mix).

N	E (eV)	PG	SA	N	E (eV)	PG	SA
				41	-199.6745	C_s	mix
2	-3.1515	$D_{\infty h}$		42	-204.9297	C_4	fsI
3	-7.3640	D_{3h}		43	-210.1853	C_2	cI
4	-12.4627	T_d		44	-215.5259	C_s	cI
5	-17.2131	D_{3h}		45	-220.6938	C_s	
6	-22.4353	O_h	fcc	46	-225.9648	C_s	cI
7	-27.2189	D_{5h}		47	-231.1459	C_s	cI
8	-31.8884	D_{2d}		48	-236.3969	C_s	cI
9	-36.7091	C_{2v}	cI	49	-241.7241	C_s	cI
10	-41.6455	C_{3v}	cI	50	-246.8295	D_{3h}	fcc
11	-46.4621	C_{2v}	cI	51	-252.1407	C_{3v}	ucI
12	-51.6089	C_{5v}	cI	52	-257.7687	C_{2h}	ucI
13	-57.5826	I_h	cI	53	-263.3864	C_{5v}	ucI
14	-61.7317	C_{3v}	cI	54	-269.0105	I_h	ucI
15	-66.9514	D_{6d}		55	-273.4541	I_h	cI
16	-71.8609	C_{2v}		56	-278.3894	C_s	
17	-76.8300	C_s		57	-283.6149	C_s	
18	-81.6960	C_{2v}		58	-288.8067	C_s	
19	-86.9222	D_{5h}	cI	59	-293.9930	C_s	
20	-91.7288	C_{2h}	fsI	60	-299.3716	C_s	
21	-96.8290	C_s	fsI	61	-304.8093	C_{3v}	fcc
22	-102.0877	C_s	fsI	62	-310.0821	C_s	
23	-107.2310	C_s	fsI	63	-315.4525	C_{2v}	
24	-112.1612	C_s	fsI	64	-320.8369	C_{2v}	dec(5)
25	-117.0114	C_3	fsI	65	-325.9583	C_s	
26	-122.2412	C_s	fsI	66	-331.2959	C_s	mix
27	-127.4586	C_s	fsI	67	-336.4653	C_s	
28	-132.7066	C_s	fsI	68	-341.9533	C_s	
29	-137.7405	C_2	fsI	69	-347.1607	C_s	
30	-143.0386	C_{3v}	fsI	70	-352.4811	C_s	dec(5)
31	-147.9993	C_3	fsI	71	-358.1813	C_{2v}	dec(5)
32	-153.1794	D_{2d}	fsI	72	-363.2608	C_s	mix
33	-158.2298	C_2	fsI	73	-368.7448	C_s	mix
34	-163.3569	C_s	fsI	74	-374.0287	C_{5v}	dec(5)
35	-168.7294	D_3	fsI	75	-379.7413	D_{5h}	dec(5)
36	-173.9244	C_{2v}	fsI	76	-384.6942	C_{2v}	dec(5)
37	-179.0675	C_{2v}	mix	77	-390.1332	C_{2v}	mix
38	-184.4825	O_h	fcc	78	-395.0530	C_s	mix
39	-189.4859	C_s	cI	79	-400.7173	D_{3h}	fcc
40	-194.8158	D_2	fsI	80	-405.7957	C_s	mix

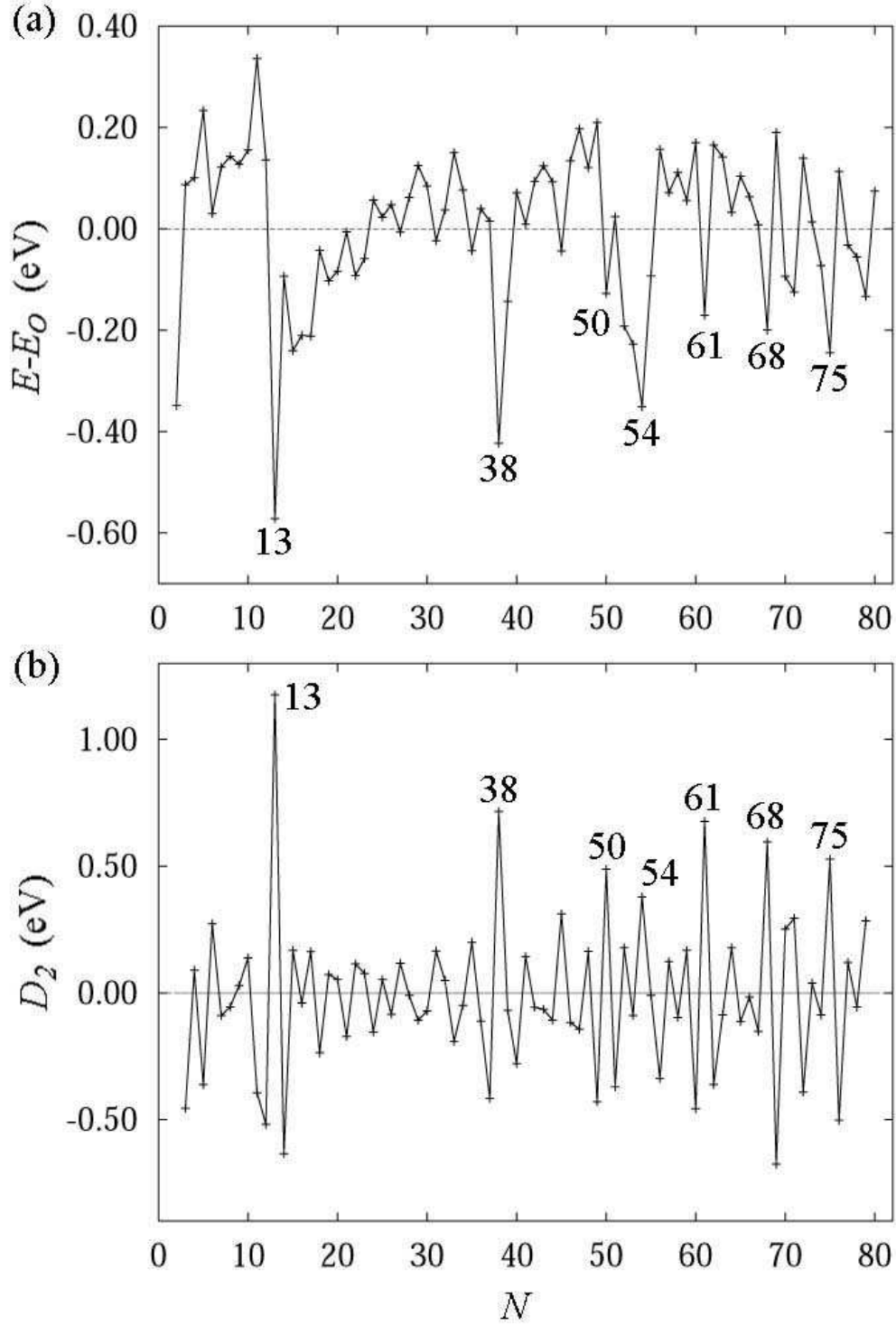


FIG. 1: (a) $E - E_0$ is the relative energies of quenched Al clusters where $E_0 = 5.09182 - 2.96861N^{1/3} + 2.7261N^{2/3} - 3.43728N$; (b) The second finite difference in binding energy v.s. size N .

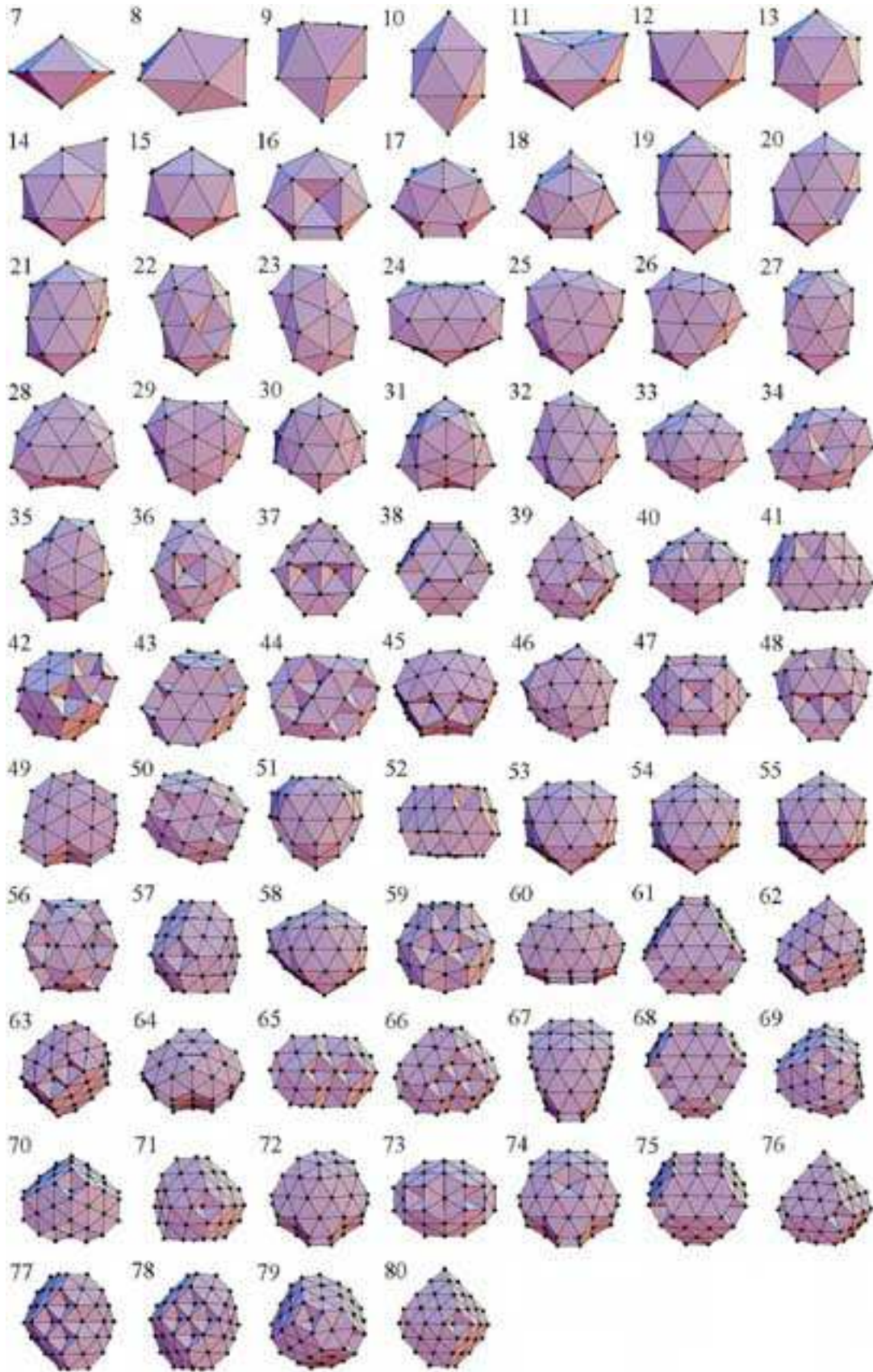


FIG. 2: Structures of the global minima for $Al_7 - Al_{80}$ clusters

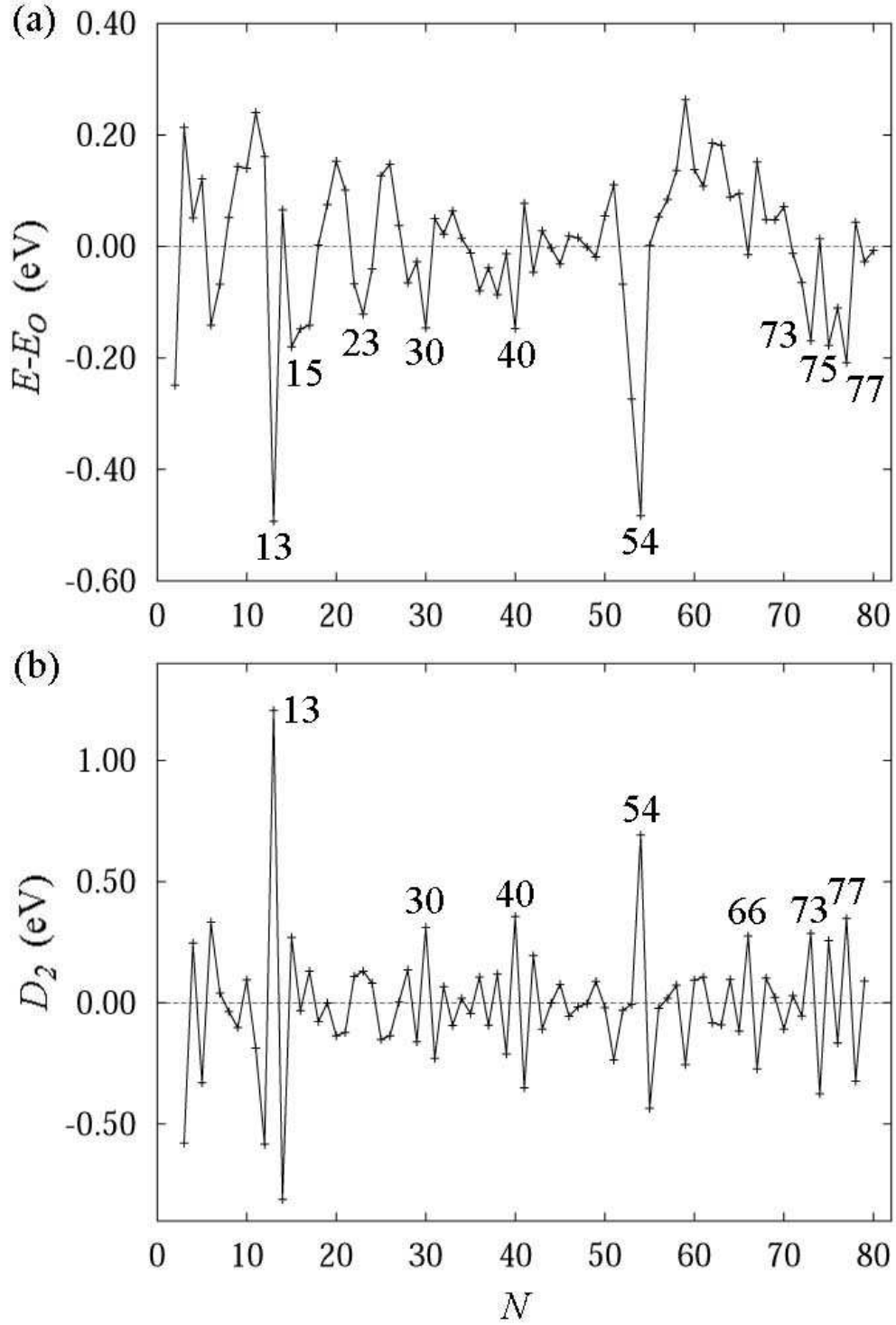


FIG. 3: (a) $E - E_0$ is the relative energies of quenched Au clusters where $E_0 = 8.63706 - 6.88748N^{1/3} + 3.97967N^{2/3} - 4.15816N$; (b) The second finite difference in binding energy v.s. size N .

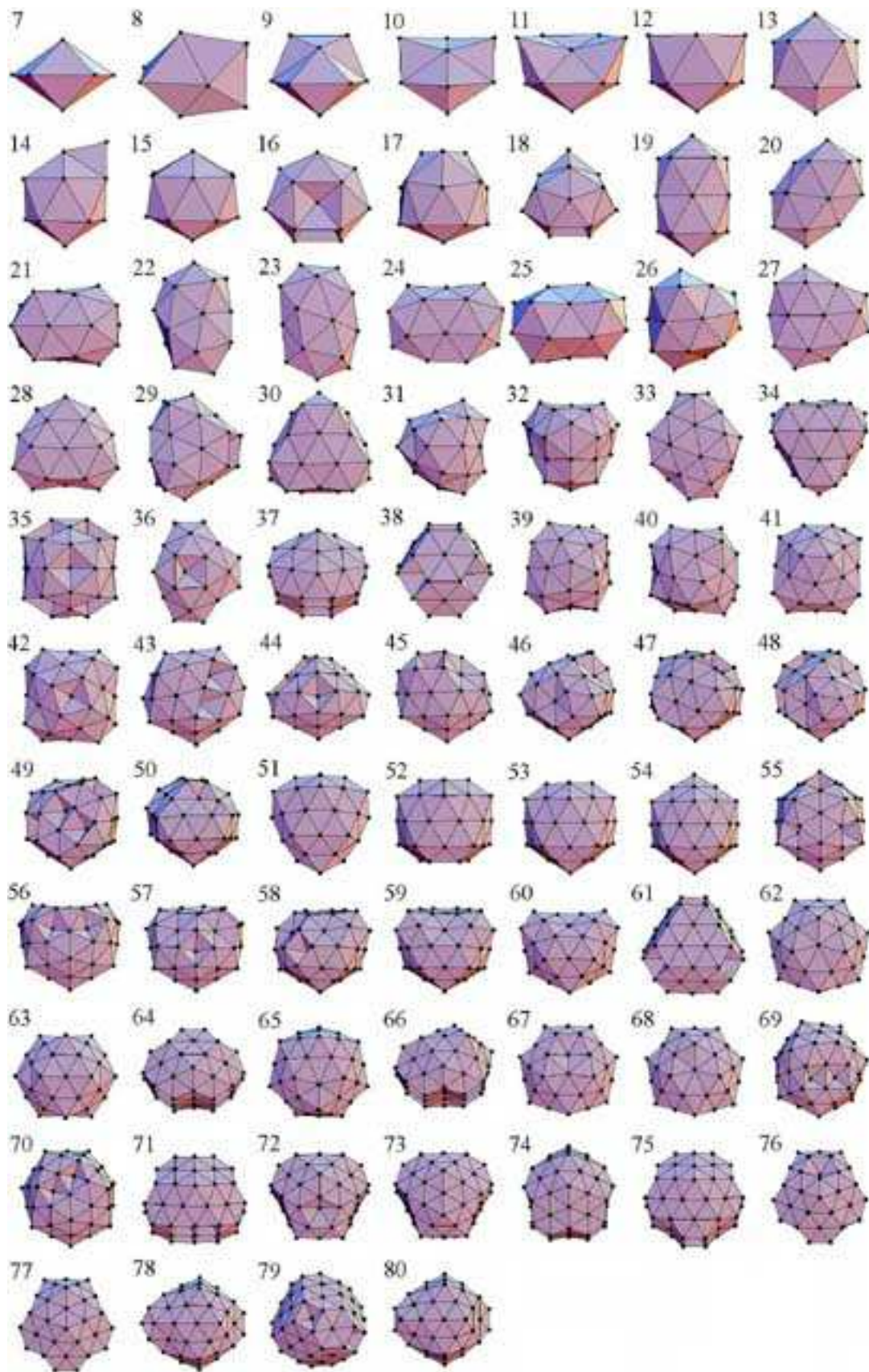


FIG. 4: Structures of the global minima for $Au_7 - Au_{80}$ clusters

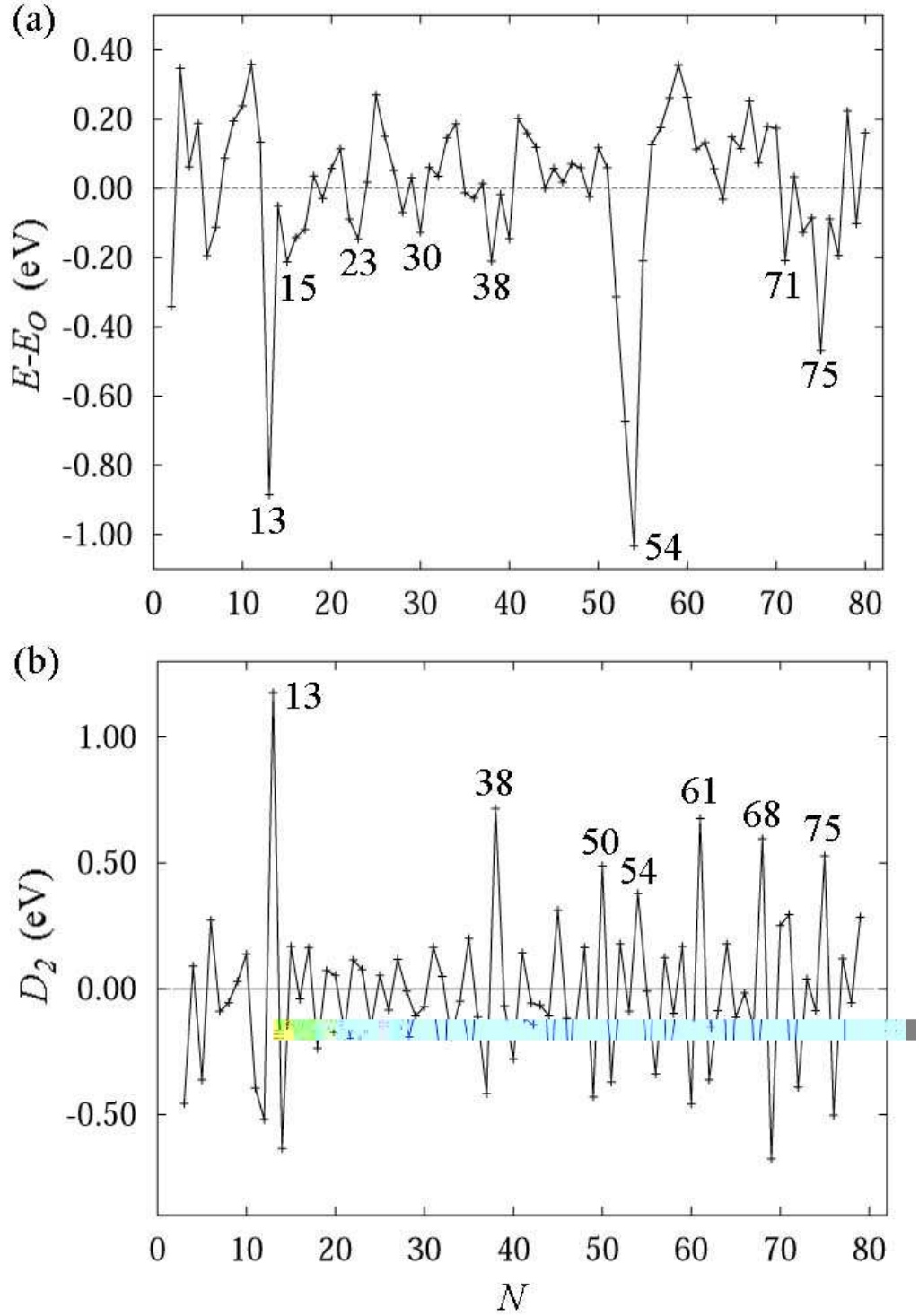


FIG. 5: (a) $E - E_0$ is the relative energies of quenched Pt clusters where $E_0 = 11.6998 - 9.27227N^{1/3} + 5.88215N^{2/3} - 6.08642N$; (b) The second finite difference in binding energy v.s. size N .

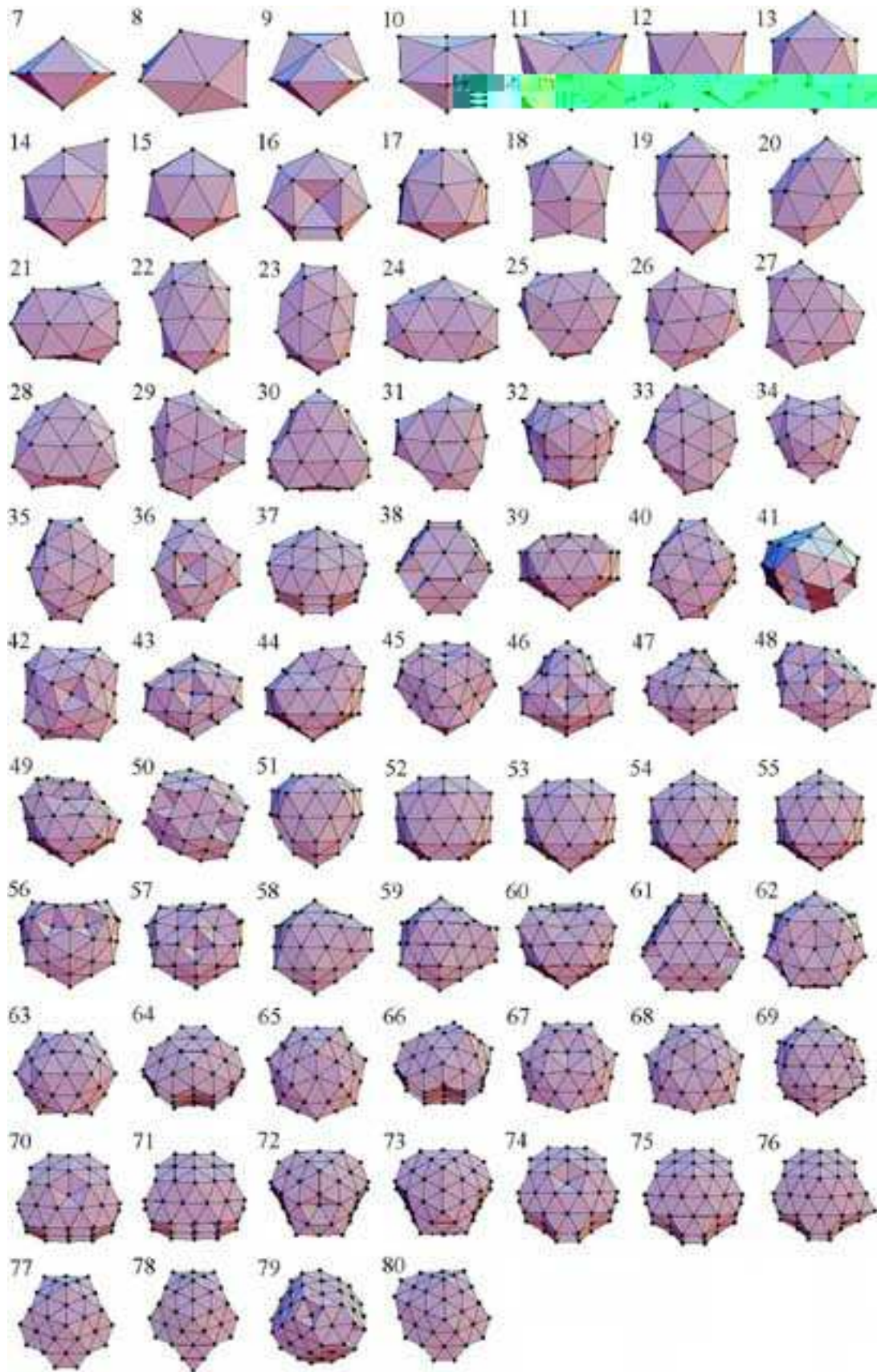


FIG. 6: Structures of the global minima for $Pt_7 - Pt_{80}$ clusters